

Simulating the impact of the large-scale circulation on the 2-m temperature and precipitation climatology

Jared H. Bowden · Christopher G. Nolte ·
Tanya L. Otte

Received: 1 February 2012 / Accepted: 26 June 2012 / Published online: 18 July 2012
© Springer-Verlag (outside the USA) 2012

Abstract The impact of the simulated large-scale atmospheric circulation on the regional climate is examined using the Weather Research and Forecasting (WRF) model as a regional climate model. The purpose is to understand the potential need for interior grid nudging for dynamical downscaling of global climate model (GCM) output for air quality applications under a changing climate. In this study we downscale the NCEP-Department of Energy Atmospheric Model Intercomparison Project (AMIP-II) Reanalysis using three continuous 20-year WRF simulations: one simulation without interior grid nudging and two using different interior grid nudging methods. **The biases in 2-m temperature and precipitation for the simulation without interior grid nudging are unreasonably large with respect to the North American Regional Reanalysis (NARR) over the eastern half of the contiguous United States (CONUS) during the summer** when air quality concerns are most relevant. This study examines how these differences arise from errors in predicting the large-scale atmospheric circulation. It is demonstrated that **the Bermuda high, which strongly influences the regional climate for much of the eastern half of the CONUS during the summer, is poorly simulated without interior grid nudging.** In particular, two summers when the Bermuda high was west (1993) and east (2003) of its climatological position are chosen to illustrate problems in the large-scale atmospheric circulation anomalies. For both summers, WRF

without interior grid nudging fails to simulate the placement of the upper-level anticyclonic (1993) and cyclonic (2003) circulation anomalies. The displacement of the large-scale circulation impacts the lower atmosphere moisture transport and precipitable water, affecting the convective environment and precipitation. Using interior grid nudging improves the large-scale circulation aloft and moisture transport/precipitable water anomalies, thereby improving the simulated 2-m temperature and precipitation. The results demonstrate that **constraining the RCM to the large-scale features in the driving fields improves the overall accuracy of the simulated regional climate, and suggest that in the absence of such a constraint, the RCM will likely misrepresent important large-scale shifts** in the atmospheric circulation under a future climate.

Keywords Regional climate modeling · Interior grid nudging · Spectral nudging · Analysis nudging · Bermuda high

1 Introduction

Regional climate models (RCMs) are frequently used for dynamical downscaling of future climate projections from global climate models to develop regional climate change impact assessments and for climate change adaptation planning. For downscaling applications in which the RCM is forced by the global fields only via the lateral boundary conditions, the large-scale atmospheric circulation simulated by the RCM can diverge from that in the driving fields. This is particularly true for large RCM domains when the synoptic forcing is relatively weak or in the tropics where there is localized convection (Wang et al. 2004).

J. H. Bowden · C. G. Nolte · T. L. Otte
U.S. EPA National Exposure Research Laboratory,
Research Triangle Park, NC, USA

Present Address:

J. H. Bowden (✉)
University of North Carolina, Chapel Hill, NC, USA
e-mail: jhbowden@unc.edu

Whether this divergence between the large-scale driving fields and the RCM solution is indicative of a problem or is a desired outcome of using a regional climate model is an open question, where the answer may depend on the specific application of interest (Giorgi 2006). Under one philosophical paradigm for dynamical downscaling, the RCM should be allowed as much freedom as possible to develop its own circulation in the interior of the modeling domain because of the potential for the RCM to provide added value. For some research applications, such as process studies of the feedback of local- or regional-scale forcings on the large-scale dynamics, the deviation between the driving fields and the regional-scale fields is the intended focus of the research, and constraining the RCM in such instances would be undesirable (Lorenz and Jacob 2005; Inatsu and Kimoto 2009). A further consideration is that global climate models have their own biases (e.g. Pielke et al. 2011), and it is possible in some situations that the RCM can improve on the atmospheric circulation present in the driving fields, even at large scales (Veljovic et al. 2010). Also, constraining the RCM could have the unintended side effect of masking the RCM model biases (Christensen et al. 2007).

An alternate philosophical paradigm of regional climate modeling is dynamical downscaling where the RCM should resolve the mesoscale circulations while retaining the GCM resolved scales of motion (Grotch and MacCracken 1991; Jones et al. 1995; Laprise et al. 2007). Various methods have been suggested to constrain the RCM to the input data: Kida et al. (1991), Waldron et al. (1996), von Storch et al. (2000) for spectral nudging methods; Lo et al. (2008) for frequent reinitialization; Bowden et al. (2012) for analysis nudging methods; Yhang and Hong (2011) for scale-selective bias correction. Recently, Bowden et al. (2012) conducted annual simulations using the Weather Research and Forecasting (WRF) model to show that persistent biases in simulated climatology can occur over large spatial regions in the absence of interior nudging, and that application of two different nudging techniques improved the accuracy of the downscaled climatology.

We extend the work of Bowden et al. (2012), which used annual simulations, by conducting multi-decadal hindcast regional climate model simulations using a global reanalysis as the driving input fields. Using the multi-decadal simulations allows us to address the RCM's ability to retain the climatological large-scale atmospheric circulation without interior grid nudging. The goal is to investigate if inconsistencies in regional climatology, as represented by errors in 2-m temperature and precipitation, are associated with misrepresentation of the large-scale circulation. Only a few studies have used long continuous integrations, which are needed to reduce model internal

variability (Alexandru et al. 2007; Lucas-Picher et al. 2008) to investigate the large-scale atmospheric circulation deviations within RCMs from the driving lateral boundary conditions. Sanchez-Gomez et al. (2009) addressed the problem of simulating the large-scale circulation for Europe with an ensemble of simulations from different RCMs. Using weather regimes, recurrent and spatially defined weather patterns (order of a few days to a few weeks), they found that the RCMs reproduced the weather regimes behavior in terms of composite pattern, mean frequency of occurrence and persistence reasonably well, indicating that the large-scale circulation was well represented within the RCMs. On the contrary, Yhang and Hong (2011) used a 26-year continuous integration to demonstrate problems in simulating large-scale atmospheric circulation and the resulting impact on the simulated precipitation. They found that using a scale-selective bias correction helped to reduce errors in the monsoon circulation, but there was no discernible advantage of using the scale-selective bias correction for precipitation. This study helps to provide further insight into the large-scale atmospheric circulation simulated within RCMs by showing robust examples of the impact of the large-scale atmospheric circulation on simulated 2-m temperature and precipitation. Additionally, this study is the first to compare the RCM simulated atmospheric large-scale circulation using two different interior grid nudging techniques.

The rest of this paper is organized as follows. The model setup and experiment design are described in Sect. 2. In Sect. 3 we evaluate the biases in monthly and regionally averaged quantities over the simulation period and identify summertime in the Southeastern United States as a season and region that, in the absence of interior nudging, is frequently simulated poorly. In Sect. 4 we relate the errors in simulated summer climatology in the Southeast to the large-scale atmospheric circulation. We conclude the paper with a concise summary and future research needs.

2 Model description and experiment design

The WRF model (Skamarock et al. 2008) is a fully compressible, non-hydrostatic model that uses a terrain-following vertical coordinate. In this study, WRF is run using a 34-layer configuration extending to a model top at 50 hPa. A two-way interactive nest is used with horizontal grid spacings of 108 km (81×51 grid points) covering most of North America and 36 km (187×85 grid points) over the contiguous United States (CONUS), as shown in Fig. 1. We use WRF version 3.2.1 with physics options including the Community Atmospheric Model for longwave and shortwave radiation (CAM; Collins et al. 2004), the WRF single-moment six-class microphysics scheme

(Hong and Lim, 2006), the Grell ensemble convective parameterization (Grell and Dévényi 2002), the Yonsei University planetary boundary layer (PBL) scheme (Hong et al. 2006), and the Noah land-surface model (Chen and Dudhia 2001). The simulations use time-varying sea-surface temperature, sea ice, vegetation fraction, and albedo.

WRF is used to downscale $2.5^\circ \times 2.5^\circ$ analyses from the NCEP-Department of Energy Atmospheric Model Intercomparison Project (AMIP-II) Reanalysis (Kanamitsu et al. 2002) (hereafter, R-2) for the period 1988–2007. The model is initialized at 00 UTC 02 Dec 1987, allowed to spin up for one month, and integrated continuously to 00 UTC 01 Jan 2008. In these runs, the R-2 fields serve as proxies for data from a global climate model. However, the R-2 fields represent the best available representation of the meteorology that occurred at the 2.5° spatial scale for that historical period, so can be regarded as “perfect boundary conditions” (Christensen et al. 1997). The R-2 fields provide initial, lateral, and surface boundary conditions, and they serve as the constraints for interior nudging used in this paper. No observational data exogenous to the R-2 fields are assimilated for any of the simulations.

Two methods of interior grid nudging have been implemented in WRF. Both forms of interior nudging can reduce mean errors in regional climate modeling with WRF (e.g., Lo et al. 2008; Bowden et al. 2012). Analysis nudging (Stauffer and Seaman 1994) is theorized to be most useful when the input data fields are not significantly coarser than the model resolution. In analysis nudging, the prognostic equations are modified by adding a non-physical term proportional to the difference between the model state and a value that is interpolated in time and space from the reference analysis. Spectral nudging (von Storch et al.

2000; Miguez-Macho et al. 2004) is attractive as a scale-selective interior constraint for dynamical downscaling because it is applied only to wavelengths longer than a specified threshold. In WRF, analysis nudging can be applied toward horizontal wind components, potential temperature, and water vapor mixing ratio, while spectral nudging is available for horizontal wind components, potential temperature, and total geopotential. When either analysis or spectral nudging is used, it is applied only above the PBL to maximize WRF’s freedom to respond to mesoscale forcing within the PBL.

Three 20-year simulations are conducted. All simulations apply the R-2 boundary conditions using a 5-cell-width relaxation zone (Davies 1976). The first simulation, NN, uses no interior grid nudging; the second, AN, uses analysis nudging; and the third, SN, uses spectral nudging. The nudging coefficients and wave numbers used for analysis and spectral nudging are as specified in Table 1.

3 Evaluation of biases in simulated climatology

Validating the atmospheric circulation in RCMs is difficult for large domains because atmospheric processes have non-uniform impacts on the regional climatology within the domain. Several approaches have been used to understand the large-scale circulation within RCMs. For instance, focus could be placed on large-scale circulation mechanisms that impact the regional climatology, e.g., atmospheric rivers and flooding for the Northwest United States (Leung and Qian 2009). Other approaches are mainly statistical, such as using cluster analysis to group weather patterns based on the distribution of certain atmospheric

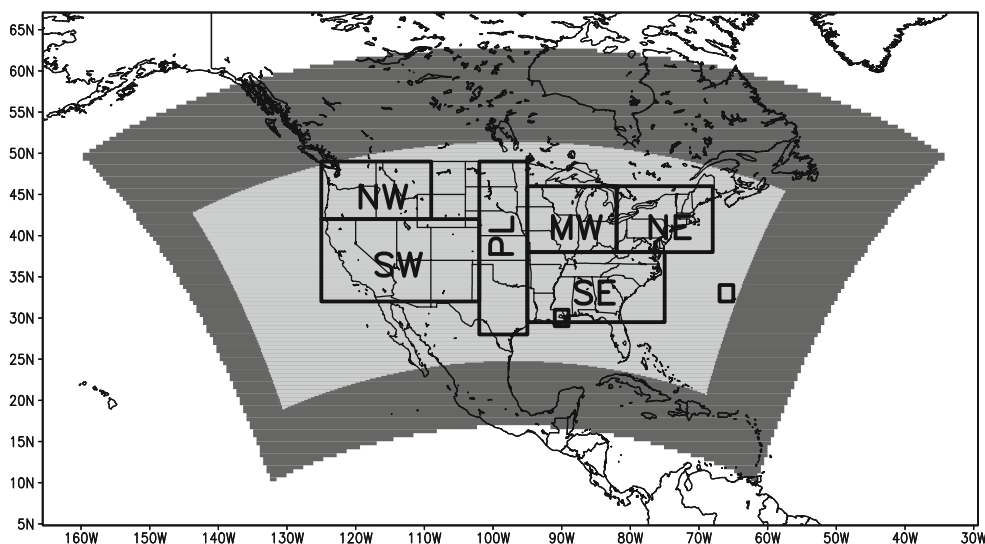


Fig. 1 WRF outer (108-km) and inner (36-km) domains. Box regions used for model evaluation: Northwest (NW), Southwest (SW), Plains (PL), Midwest (MW), Southeast (SE), and Northeast (NE). Also shown are the boxes used to define Bermuda and New Orleans in calculating the BHI

Table 1 Nudging coefficients (s^{-1}) and domain-relative wave numbers used for analysis and spectral nudging simulations

	Wind	Potential Temp.	Water vapor mixing ratio	Geopotential	West-east wave number	South-north wave number
Analysis nudging (108-km)	3.0×10^{-4} (0.9)	3.0×10^{-4} (0.9)	4.5×10^{-5} (0.9)	–	–	–
Analysis nudging (36-km)	1.0×10^{-4} (2.8)	1.0×10^{-4} (2.8)	1.0×10^{-5} (27.8)	–	–	–
Spectral nudging (108-km)	3.0×10^{-4} (0.9)	3.0×10^{-4} (0.9)	–	3.0×10^{-4} (0.9)	5 (1728)	3 (1800)
Spectral nudging (36-km)	3.0×10^{-4} (0.9)	3.0×10^{-4} (0.9)	–	3.0×10^{-4} (0.9)	4 (1674)	2 (1512)

Time scales (h) that correspond to the nudging coefficients and length scales (km) that correspond to the wave numbers are in parentheses. Fields that are not applicable are indicated by –

variables (Robertson and Ghil 1999; Sanchez-Gomez et al. 2009).

Here, the analysis is focused on surface-based meteorology that is directly linked to the atmospheric large-scale circulation. For each month in the 20-year time series, we compute monthly- and area-averaged 2-m temperature and precipitation over land grid cells for six regions of the CONUS, Fig. 1. These fields are chosen because of their fundamental importance for climate change impact assessments. The 36-km WRF simulations are evaluated against the 32-km North American Regional Reanalysis (NARR; Mesinger et al. 2006), where the NARR data are bilinearly interpolated to the 36-km WRF domain. The NARR 2-m temperature and precipitation data have been found to compare well with observations over land within the CONUS (Mesinger et al. 2006; Nigam and Ruiz-Barradas 2006) and have been used in several previous RCM model validation studies (Lo et al. 2008; Bukovsky and Karoly 2009; Bowden et al. 2012). Additionally, we calculate the area average difference between NARR and R-2 over land because important biases between NARR and R-2 will impact the nudged simulations.

The mean biases in 2-m temperature for the 20-year period are plotted by month in Fig. 2 for each of the evaluation regions. With this model configuration, an overall cool bias exists for all three simulations. The annual average bias over the CONUS is -2 K for the NN simulation. For the Midwest, Northeast, and Southeast the mean error in the NN simulation typically exceeds -3 K. Biases of this magnitude may pose a serious limitation for climate change impact assessments because regional climate change projections may have the same magnitude of change (Giorgi 2006); however, biases may not impact the climate change signal if the model biases are conserved between current and future climates. The bias between R-2 and NARR is small over regions with large errors east of the Rockies in the NN simulation, further justifying

nudging to R-2. Considering all regions, the largest average monthly error occurs in the Northeast during August, where the average bias is -5.2 K. When either interior grid nudging technique is used, the mean annual bias across the CONUS improves to -1 K. With the exception of the Southwest, both AN and SN reduce the mean regional 2-m temperature error. Note that this region also has a large difference between NARR and R-2 demonstrating biases in the driving data impact the RCM bias. Specifically, notable differences between NARR and R-2 are found over regions with complex terrain.

Regionally averaged biases in the monthly accumulated precipitation are shown in Fig. 3. Averaged over the CONUS, the NN simulation has an annual wet bias of about 12 mm month $^{-1}$. However, there is a strong seasonal variation to the precipitation bias. The bias decreases during the summer to late fall throughout the CONUS, becoming negative for all regions except for the Northwest, which mitigates the positive bias in the annual average. The AN simulation has the smallest bias of 9 mm month $^{-1}$ averaged over the CONUS, while the SN simulation has the largest wet bias of 21 mm month $^{-1}$. Although SN is wetter than AN, the month-to-month bias is correlated between the AN and SN simulations, exceeding 0.8 for all regions with the exception of the Northwest. The high correlation suggests that the two nudging techniques are behaving similarly. The difference in the magnitude of the precipitation bias between the nudged simulations may be because the water vapor mixing ratio is nudged in AN but not in SN. A notable difference in AN and SN relative to NN is the switch in sign of the bias over the Southeast extending into the Northeast region during the summer months (JJA). The AN and SN simulations have a wet bias during the summer for the Southeast with an average of 23 mm month $^{-1}$ compared to a dry bias exceeding 30 mm month $^{-1}$ for the NN simulation. There is also a switch in sign of the bias for AN and SN during July and August

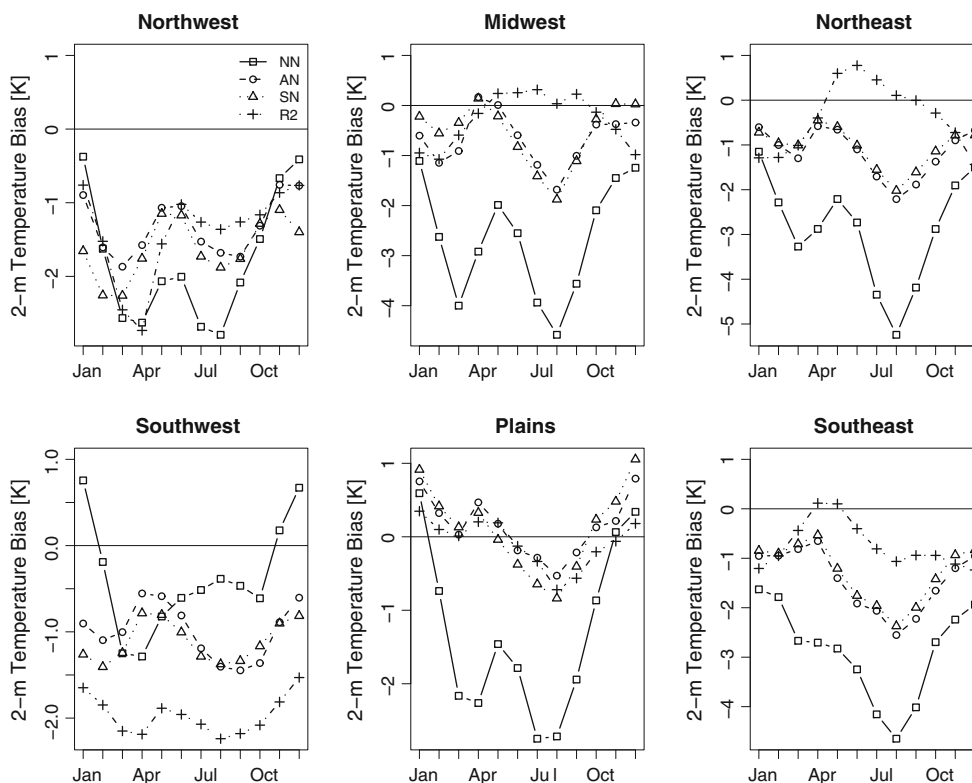


Fig. 2 Mean monthly-averaged 2-m temperature bias (K) relative to NARR for each of the six verification regions shown in Fig. 1 for R-2 (plus-dot-dash), NN (square-solid), AN (circle-dash), and SN (triangle-dot)

compared to NN with a large positive precipitation bias for both AN and SN during the summer.

Next, for each region in the NN simulation we identify the months with absolute errors in the top 10 % for the 20-year period (i.e., the 24 highest monthly errors) by boreal season (Figs. 4, 5). The largest errors in 2-m temperature in NN most frequently occur during the summer in five of the six regions (Fig. 4). The incidences of large errors in 2-m temperature are greatest in the Northeast and Southeast (75 and 66 %, respectively) which are the regions that are farthest from the inflow boundary.

Figure 5 is similar to Fig. 4 but for precipitation, and it illustrates that the season during which the largest NN precipitation errors occur varies widely across the CONUS. For instance the Northwest region has 14 of the 24 (58 %) largest biased months occurring during the boreal winter, while in the Southeast a plurality of the largest errors occur during the summer. The winter bias in the Northwest is clearly related to the seasonal cycle and when the majority of precipitation occurs. However, the Southeast has a more even climatological distribution of rainfall throughout the year.

These results for the temperature and precipitation biases provide motivation to understanding the extent to which errors in WRF are related to errors in simulating the

atmospheric circulation over the eastern half of the US, in particular the Southeast, during the summer.

4 Evaluation of atmospheric circulation errors

Our focus for this dynamical downscaling research is assessing the impact of regional climate change on air quality in the United States. Substantial errors in the NN simulation during the summer in the Southeast (when air quality is most problematic) present a significant problem and may adversely impact the reliability of the RCM output for the air quality application. The regional climate variability during the summertime over the Southeast is associated with several factors, including hurricanes (Liu and Fearn 2000), soil moisture (Koster et al. 2004), and atmospheric circulation anomalies associated with changes in sea surface temperatures (Wang and Enfield 2001; Seager et al. 2003). In particular, the atmospheric circulation related to the position of the Bermuda high has a major impact on the regional climate and air quality for the Southeast. The position of the Bermuda high has shifted westward and become more intense in recent decades and is projected to shift further west and become more intense by GCMs as the climate warms (Li et al. 2010). RCMs that are unable to simulate the position and intensity of the Bermuda

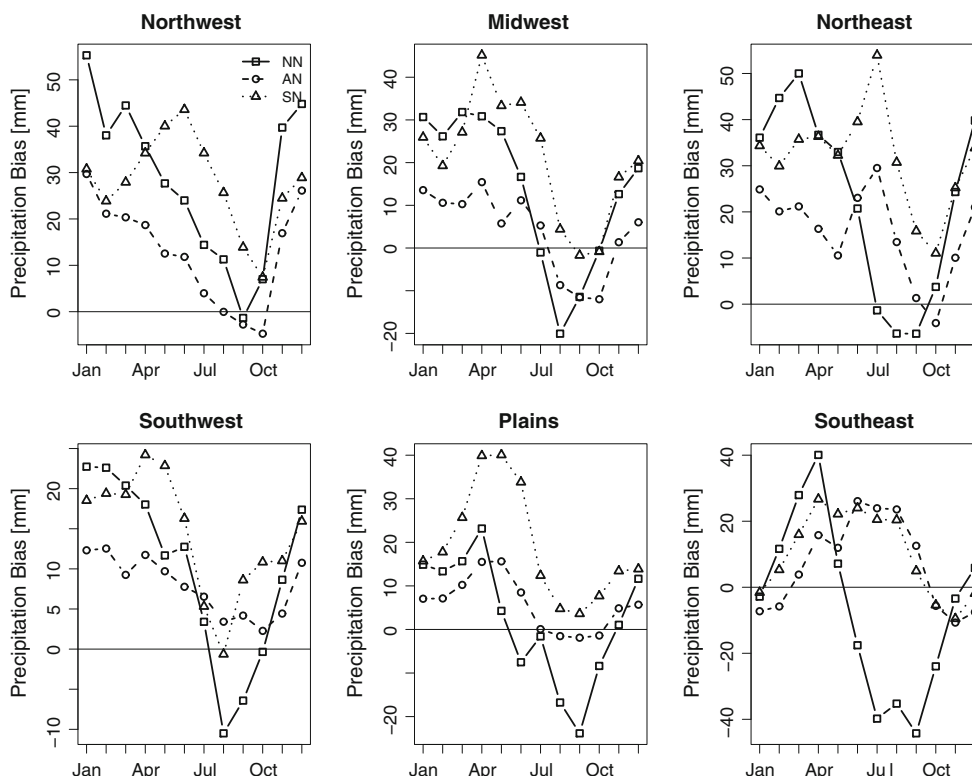
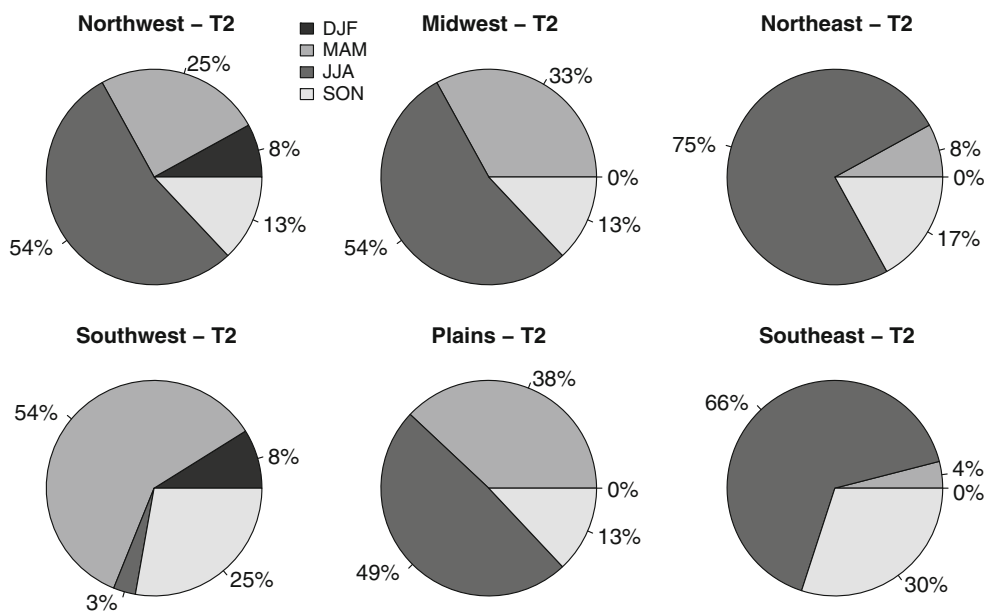


Fig. 3 Mean monthly-averaged 2-m precipitation bias (mm month^{-1}) relative to NARR for each of the six verification regions shown in Fig. 1 for NN (square-solid), AN (circle-dash), and SN (triangle-dotted)

Fig. 4 Seasonal distribution for NN of the top 10 % highest errors in monthly-averaged temperature for each of the six regions shown in Fig. 1. Each shade represents a different season



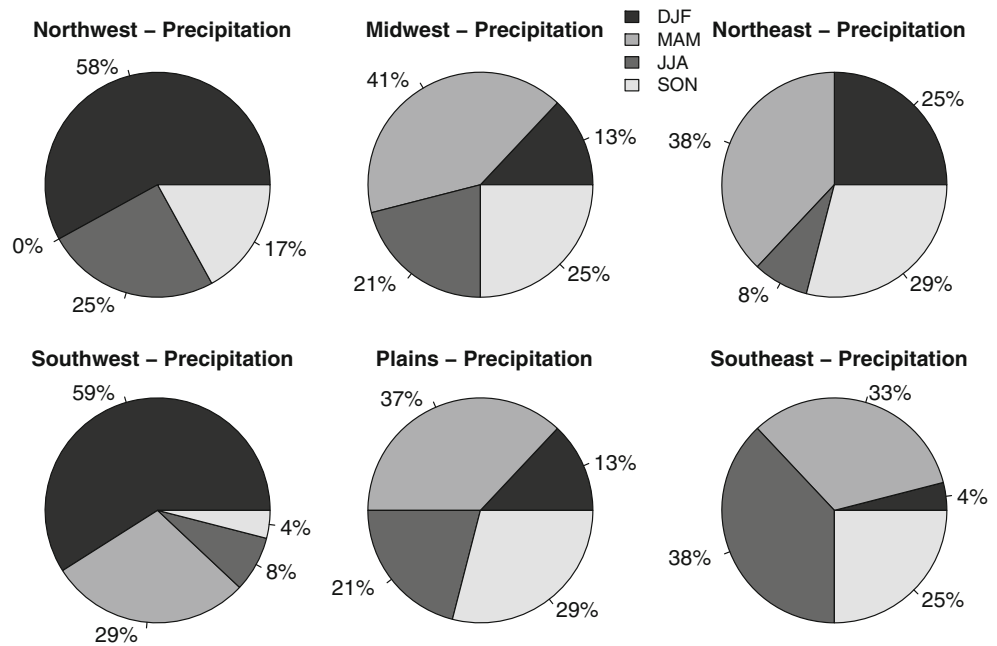
high under current climate are unlikely to properly simulate climate change impacts, such as for future air quality.

4.1 Bermuda high index

The location and intensity of the Bermuda high during the contemporary climate are examined for the RCM

simulations using the Bermuda High Index (BHI; Katz et al. 2003). The BHI measures the western extent of the Bermuda high by using the climatologically normalized difference in boreal summer (JJA) sea-level pressure between Bermuda and New Orleans (Katz et al. 2003). Because Bermuda is located close to our lateral boundary, we adopt a modified approach using area averages for both

Fig. 5 Seasonal distribution for NN of the top 10 % highest errors in monthly-averaged precipitation for each of the six regions shown in Fig. 1. Each shade represents a different season



regions. “Bermuda” is the region between 67°–65°W and 32°–34°N and “New Orleans” is the region between 91°–90°W and 29°–31°, Fig. 1. Positive and negative BHI values indicate that the Bermuda high is further east and west than normal, respectively. To calculate the BHI, the monthly sea-level pressure is first normalized at all grid points:

$$SLPnorm_{xy}(mon) = \frac{SLP_{xy} - \overline{SLP}_{xy}}{\sigma_{SLP_{xy}}} \quad (1)$$

The normalized monthly values are then averaged over JJA for the regions and subtracted to give the BHI:

$$BHI = \frac{1}{np} \sum_{i=1}^{np} \left[\frac{1}{3} \sum_{t=1}^3 SLPnorm_{xy}(t) \right]_{be} - \frac{1}{np} \sum_{i=1}^{np} \left[\frac{1}{3} \sum_{t=1}^3 SLPnorm_{xy}(t) \right]_{no} \quad (2)$$

where np is the number of grid points for Bermuda (be) and New Orleans (no), and the average is taken over three summer months.

The BHI is calculated for the R-2, NARR and the WRF simulations. In this analysis, the BHI quantifies WRF’s ability to properly simulate the Bermuda high intensity and location without and with interior nudging. In addition, the BHI is used to identify years when the Bermuda high is poorly simulated without interior grid nudging to understand how the errors in the large-scale circulation are related to errors in regional climate anomalies.

In Fig. 6, the BHI from the NARR, R-2, and the WRF simulations are compared to examine WRF’s ability to

capture the interannual variability in the intensity and position of the Bermuda high during the contemporary climate. The BHI correlation between NARR (R-2) and NN is 0.12 (0.11), while the correlation drastically improves to 0.98 (0.82) for both AN and SN, respectively. The poor correlation between the NARR data and NN suggests a deficiency in capturing the large-scale circulation, and it raises some questions. How does the misrepresentation of the Bermuda high impact the regional climate anomalies of interest to many end-user applications? How is the large-scale circulation different from the observations when no nudging is used? Can interior grid nudging adjust the anomalous placement of the Bermuda high and the associated regional climate anomalies? To begin answering these questions, we use the BHI to identify two summers from the 20-year period when the Bermuda high was west/east of its climatological average position and poorly simulated in the NN simulation. Figure 6 indicates that the most anomalous positions of the Bermuda high during this 20-year period are 1993 (west) and 2003 (east), which are both poorly represented in the NN simulation. Below we discuss the temperature and precipitation anomalies and the corresponding large-scale atmospheric circulation from all simulations and observations for 1993 and 2003. The anomalies for each model are relative to the 20-year average values (i.e., climatology) during the summer for that model.

4.2 Temperature anomalies

We first explore the impact of the placement of the Bermuda high on the regional climate anomalies for 2-m

temperature. During 1993 the observed BHI is negative (based on NARR), indicating a westward shift in the Bermuda high. This westward shift, centered closer to the eastern United States, favors warm anomalies for the Southeast, as shown in Fig. 7a. In the 1993 JJA observations, there is a corridor of warm anomalies ($>0.7\text{K}$) extending from Texas northeast into West Virginia. The warm anomalies over the Southeast are surrounded by -1.5K cool anomalies in the Midwest and northern Plains regions and as large as -1.0K over the Atlantic Ocean. An important signature in the temperature anomalies is their wavelength as indicated by their change in sign, which is on the order of 1,000 km. A wavelength with this magnitude indicates a shift in the synoptic scale atmospheric circulation. By contrast, in 2003 the BHI is positive, which indicates the center of the high is shifted east of its climatological average position. In 2003 the temperature anomalies are negative for most of the Southeast and the Midwest (Fig. 7e). The cool anomalies have approximately the same magnitude as the warm anomalies in 1993, -0.7K . As in 1993, there is a signature of a shift in the synoptic circulation with warm anomalies to the west and east of the cool anomalies. Capturing the temperature anomalies in the eastern US during 1993 and 2003 could indicate the model's overall ability to simulate the large-scale atmospheric circulation.

For JJA in 1993, all three model runs correctly simulate a warm anomaly over much of the eastern half of the US, but the placement and magnitude of the anomalies differs between the simulations (Fig. 7b–d). Tables 2 and 3

illustrate that both AN and SN improve the RMSE and pattern correlation over NN for the 1993 temperature anomalies. In particular, the temperature anomalies for 1993 in NN cover a much larger area that is centered much farther west towards southern Missouri and Illinois than in NARR, and they are warmer than observations by more than 1 K in some locations. Additionally, the temperature anomalies are of the opposite sign in some areas. Despite the disagreement in placement and sign, the warm anomalies are surrounded by anomalies of the opposite sign, as in the observations. The AN temperature anomalies are in better agreement with the observations than NN, but the warmest anomalies are in central Tennessee, west of the observations. However, the transition from warm to cool anomalies, such as in central Missouri and the western Atlantic, is well simulated by AN. That transition is also well simulated in SN, but the magnitude of the warm anomalies is much larger than observed and even further west into northern Texas and Oklahoma for the SN simulation. Overall, the AN and SN 2-m temperature anomalies, and their gradients, suggest that the large-scale atmospheric circulation shift is well captured, but local processes are simulated differently between the two types of nudging techniques.

For 2003 and as in 1993, all three simulations correctly predict the sign of the anomaly over the eastern half of the US, but the placement and magnitude of the anomalies differ greatly (Fig. 7f–h). In the NN simulation, the strongest cool anomalies are farther north towards the Great Lakes and are much cooler, 0.5 K cooler than

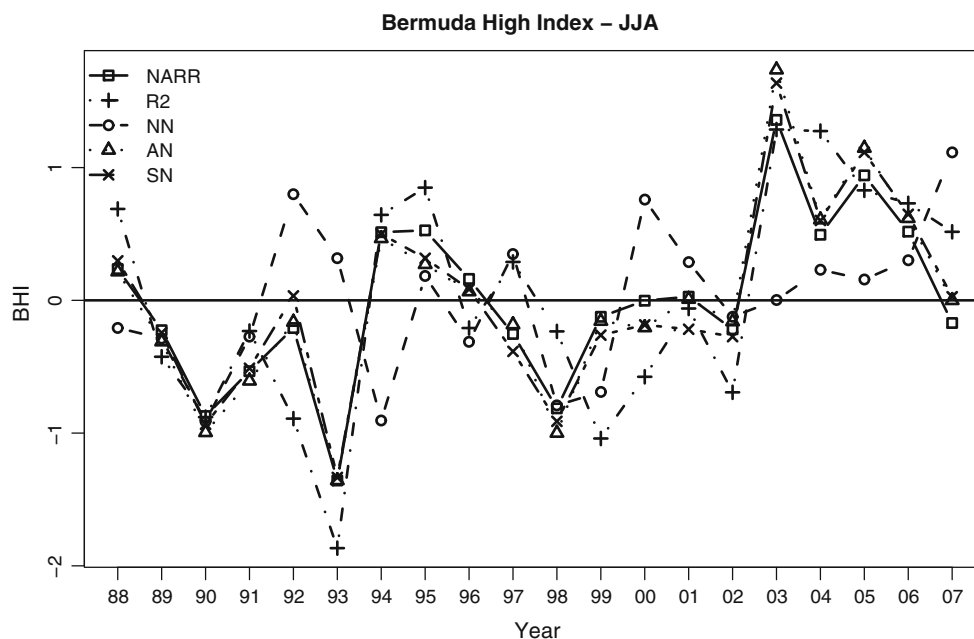
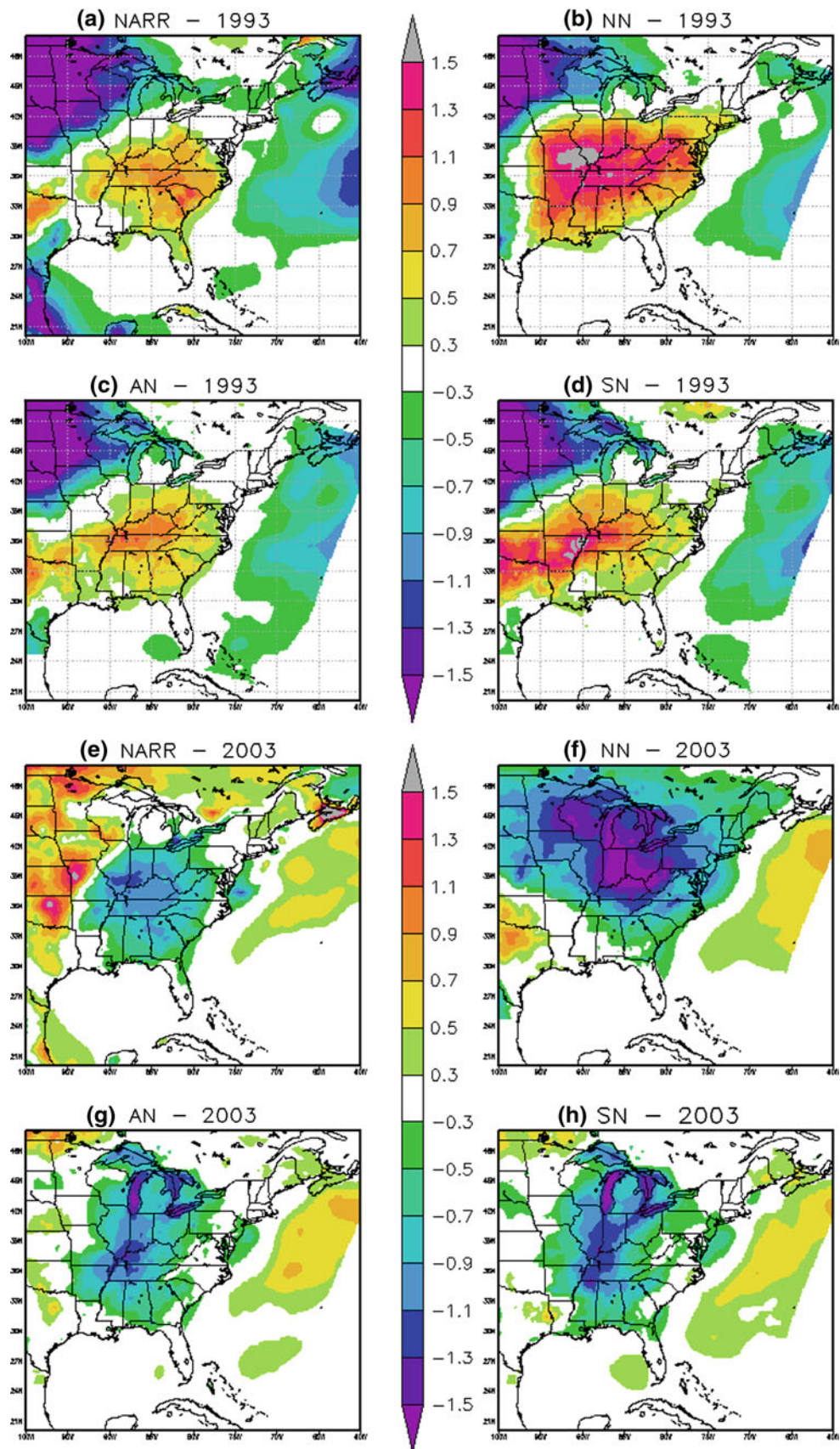


Fig. 6 Bermuda High Index calculated for the boreal summer season for NARR (square–solid), R-2 (plus–dot–dash), NN (circle–dash), AN (triangle–dot), and SN (x–dash–dot)

Fig. 7 2-m temperature anomaly (K) averaged for the summer season for 1993 (*top 4 panels*) and 2003 (*bottom 4 panels*). The panels are labeled **a** NARR, **b** NN, **c** AN, **d** SN, **e** NARR, **f** NN, **g** AN, and **h** SN



observations. The pattern correlation (Table 3) is only 0.27, indicating problems in simulating the placement of the temperature anomalies, while the RMSE of 1.1 K (Table 2) indicates problems in simulating the magnitude of the anomalies. NN indicates a shift in the synoptic circulation, with warm anomalies surrounding the cooler anomalies over the eastern US; however, there are large areas with differences in sign of the anomalies, such as the northern Midwest and central/northern Plains regions. In both AN and SN, the placement and magnitude of the cool anomalies is generally well simulated, with pattern correlation increasing to 0.74 and a decrease in the RMSE by as much as 0.6 K. The warm anomalies over the Atlantic are also well captured in AN and SN, but the warm anomalies over the Plains are largely absent in both nudging cases. The absence of these warm anomalies, which cover a large area, may reflect reduced accuracy of the large-scale atmospheric circulation simulated by both AN and SN.

4.3 Precipitation Anomalies

The observed negative precipitation anomalies over the Southeast for 1993 (Fig. 8a) are intuitively consistent with a westward shift in the Bermuda high towards the CONUS. The dry conditions extend from Texas across the Southeast and into the Northeast. The largest negative precipitation anomalies are centered over northern Georgia and western North Carolina and coincide with some of the largest positive 2-m temperature anomalies. Consistent with the temperature field and a shift in the large-scale atmospheric circulation, there is a change in the sign of the precipitation anomalies towards the Midwest and northern Plains region. The year 1993 is well known for the devastating flooding that occurred over this region, as suggested by anomalies $>100 \text{ mm month}^{-1}$ (Fig. 8a). Trenberth and Guillemot (1996) discuss some of the large-scale circulation processes involved during the 1993 Midwest flood, including a southward shift in the jet stream and strong moisture transport from the Gulf of Mexico. RCMs have been used to investigate the processes related to the 1993 flood (Pal and Eltahir 2002) and as a benchmark for model performance (Anderson et al. 2003). These studies have shown soil moisture and the timing of precipitation associated

with mesoscale convective systems were important in simulating the 1993 flood. However, the RCM must also accurately simulate the large-scale circulation, which is responsible for moisture flux into this region. Accordingly, the summer of 1993 is ideal for relating problems in the simulated temperature and precipitation anomalies to the large-scale circulation anomalies.

In 2003, with the Bermuda high east of its climatological position, positive precipitation anomalies are evident over the Southeast (Fig. 8e). The wet conditions extend as far north as Pennsylvania, with the largest positive precipitation anomalies concentrated along the Gulf Coast. There is also a dry bias in the central and northern Plains region. The 1993 and 2003 precipitation anomalies are of the opposite sign, as with temperature, indicating a shift in the synoptic-scale atmospheric circulation. An exception is over the ocean where the NARR precipitation anomalies are of the same sign between 1993 and 2003, but the confidence in NARR precipitation is low over the ocean because there are few observations available for assimilation.

The 1993 precipitation anomalies for the NN, AN, and SN simulations are shown in Fig. 8b, c, and d, respectively. Though NN indicates that summer 1993 is drier than average for the Southeast, the magnitude and extent of the Southeast drought are not captured. Furthermore, the precipitation anomalies in Texas, Florida, and Georgia have the wrong sign. Finally, the rainfall responsible for the Midwest flooding is poorly simulated, with the positive precipitation anomalies in NN located in Minnesota and South Dakota, several hundred kilometers to the northwest of the observed location. The AN simulation improves the signal of dry conditions relative to NN, see Tables 2 and 3, but the Southeast drought is more intense than observed and is located to the south and east of its observed position. The precipitation anomalies associated with the Midwest flooding are well captured in AN, with the magnitude and location of the largest positive precipitation anomalies similar to observations. In SN, the Southeast drought is more intense than observed for most locations, with the largest negative anomalies centered along the Gulf Coast. The 1993 flooding for the Midwest is also captured in SN, but the westward extent of the positive precipitation anomalies (towards Nebraska) is absent, and instead there

Table 2 RMSE for 1993 and 2003 between NARR and WRF anomalies for 2-m temperature, precipitation, precipitable water, wind speed, and wind direction

	T2 (K)			Pre (mm/day)			PWAT (mm/day)			Wspd (m/s)			Wdir (°)		
	NN	AN	SN	NN	AN	SN	NN	AN	SN	NN	AN	SN	NN	AN	SN
RMSE															
1993	0.7	0.3	0.5	1.4	1.0	1.2	0.8	0.5	0.7	0.7	0.3	0.3	90	39	34
2003	1.1	0.5	0.6	1.5	0.9	1.2	1.7	0.7	1.2	2.0	0.2	0.3	170	48	35

Table 3 Pattern Correlation for 1993 and 2003 between NARR and WRF anomalies for 2-m temperature, precipitation, precipitable water, wind speed, and wind direction

	T2			Pre			PWAT			Wspd			Wdir		
	NN	AN	SN	NN	AN	SN	NN	AN	SN	NN	AN	SN	NN	AN	SN
Pattern correlation															
1993	0.82	0.96	0.92	0.35	0.85	0.66	0.81	0.93	0.88	0.88	0.98	0.98	0.47	0.91	0.93
2003	0.27	0.74	0.67	-0.19	0.60	0.40	0.14	0.87	0.70	0.29	0.96	0.93	0.05	0.88	0.85

is an eastward extension of the anomalies to Indiana and Ohio. Previous studies have demonstrated the importance of local processes such as evaporation and moisture flux (Pal and Eltahir 2002), and perhaps the large-scale circulation contribute to these differences.

Precipitation anomalies for NN, AN, and SN during 2003 are shown in Fig. 8f, g, and h, respectively. The NN 2003 precipitation anomaly is poorly simulated throughout the eastern half of the CONUS. Also, the precipitation anomaly for much of the Southeast is of opposite sign from the observations, and there are positive anomalies in the Midwest extending across central Illinois that are not observed. Both interior nudging techniques significantly improve the ability to simulate the precipitation anomalies including the RMSE and pattern correlation during 2003 (Tables 2, 3). AN captures the wet conditions across the Southeast, but locally the precipitation anomalies are 40 mm month⁻¹ larger than observed. However, the placement of the maximum precipitation anomalies along the Gulf Coast is well simulated, and AN also captures the transition to drier conditions into the Midwest and Plains regions. The SN simulation also captures wetter conditions, especially along the Gulf Coast, but the positive precipitation anomalies are stronger than observed along the eastern seaboard, from North Carolina to Connecticut. The SN simulation also does not capture the gradient to drier anomalies as well as AN does, with breaks in the negative anomalies across Iowa and Nebraska that are absent from the observations. Overall, for 1993 and 2003 the precipitation anomalies are best captured by AN, though SN provides a notable improvement over NN.

4.4 Large-scale atmospheric circulation anomalies

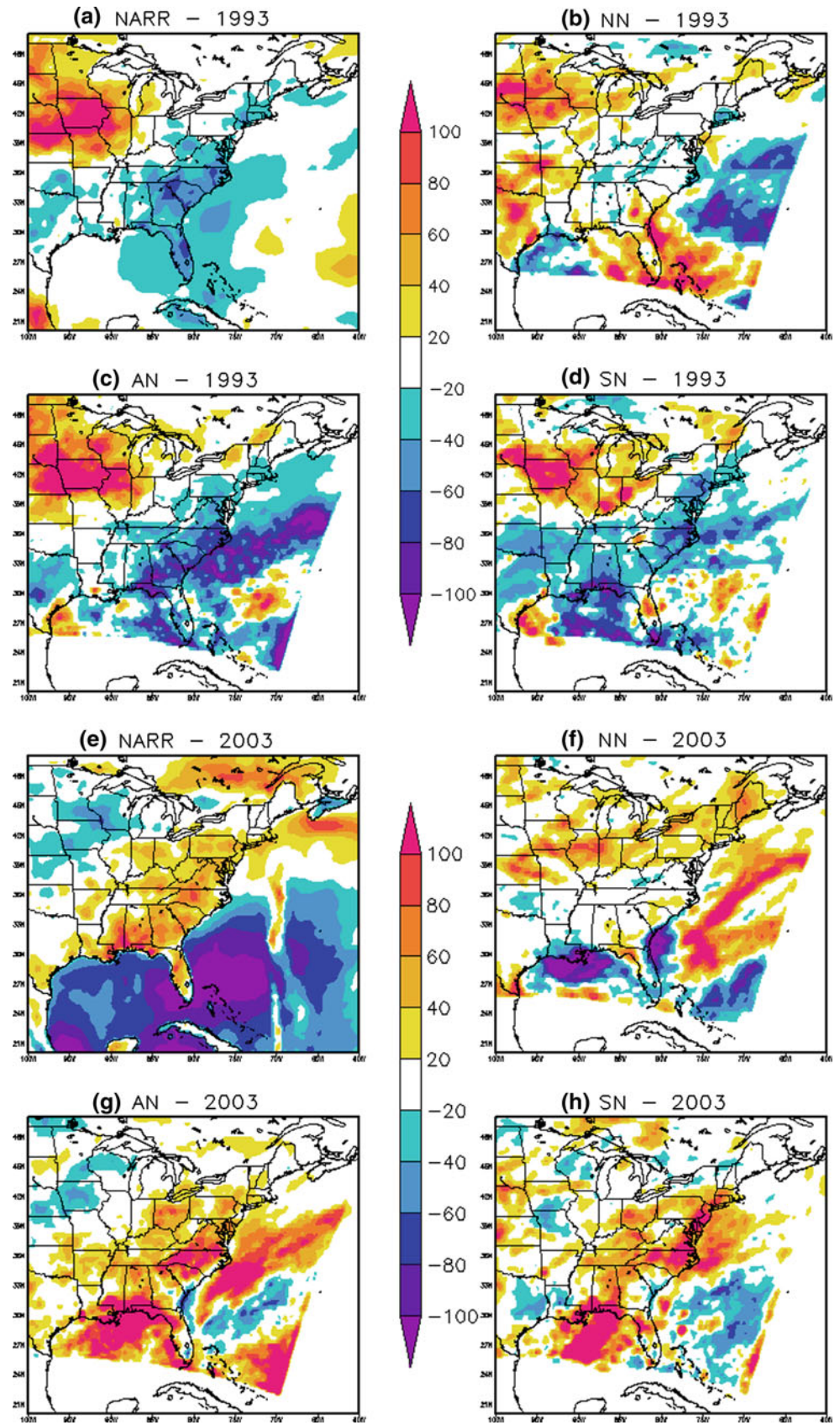
The large-scale atmospheric circulation associated with the Bermuda high consists of easterly flow over the Caribbean and a southerly jet along the eastern flanks of the Sierra Madre Oriental range. This large-scale flow favors strong moisture transport into the eastern half of the CONUS during the summer and is well represented in both the R-2 and NARR data (Nigam and Ruiz-Barradas 2006). Anomalous placement of the Bermuda high adversely

affects the large-scale atmospheric circulation and the corresponding regional climate anomalies. In this section, we examine the role of the large-scale atmospheric circulation with respect to the model simulated temperature and precipitation anomalies previously discussed. We investigate the large-scale circulation using the 500-hPa wind vector anomalies, 850-hPa moisture transport, and precipitable water anomalies for both the 1993 and 2003 summer seasons.

The summer was anomalously warm and dry in the Southeast during 1993, with cool anomalies to the west and east as shown earlier. The corresponding observed 500-hPa wind vector anomaly is shown in Fig. 9a. As anticipated from the temperature anomalies, there is a clear shift in the large-scale atmospheric circulation, with an anomalous anticyclonic circulation centered over northern Alabama and Mississippi. This anomalous anticyclonic circulation favors subsidence over the Southeast, consistent with the warm and dry anomalies and with a westward shift in the Bermuda high. Over the northern Atlantic and in northern Plains is a large anomalous cyclonic circulation consistent with the cold anomalies over the same regions. These large-scale atmospheric circulation anomalies are reversed in 2003 (Fig. 9e), with an anomalous cyclonic circulation centered over northern Kentucky and southern Indiana and Ohio, consistent with the cooler and wetter conditions over this region and extending into the Southeast. An anomalous anticyclonic circulation is found off-shore centered near the warmer anomalies. The reversal in the large-scale atmospheric circulation, temperature, and precipitation anomalies for the eastern half of the CONUS for 1993 and 2003 can be used to understand the simulated large-scale atmospheric circulation anomalies and the potential need for interior nudging toward the driving fields.

The NN, AN, and SN 500-hPa wind vector anomalies for summer 1993 are shown in Fig. 9b, c, and d, respectively. All three simulations produce an anomalous anticyclonic circulation, but in NN it is centered over Kentucky, approximately 500 km to the northeast of the observations. This displacement of the large-scale atmospheric circulation by NN causes large errors in the regional climate anomalies, as the warmest temperature

Fig. 8 Same as Fig. 7 but for precipitation anomaly (mm month^{-1})



anomalies are located to the north of the observations. AN and SN simulate the anomalous anticyclone close to its observed location compared to NN and with similar strength, and accordingly better simulate the temperature anomalies. The RMSE of the wind speed anomalies (Table 2) is reduced from 0.7 to 0.3 m s⁻¹ and pattern correlations (Table 3) increase from 0.88 in NN to 0.98 for both AN and SN. Similar conclusions can be drawn from the 2003 simulation. The 500-hPa wind anomalies for summer 2003, (Fig. 9f, g, h) all depict an anomalous cyclone over the eastern half of the US in agreement with the observations (Fig. 9e), but the location of the anomalous cyclone in NN was twice as strong as observed and was centered approximately 500 km northeast of where it occurred in the observations. This is consistent with large errors in both the wind speed and direction for 2003 as the wind speed and wind direction errors are largest during 2003 for the NN simulation (see Tables 2 and 3). The incorrect placement and strength of the cyclonic anomaly in NN leads to large errors in the regional placement of temperature anomalies for much of the eastern half of the US, with anomalies too cold in the Great Lakes area to the north and not cold enough over the Southeast. The AN and SN simulations improve the representation of the anomalous cyclone location and strength in 2003, with significant improvements in the wind speed and direction as seen in Tables 2 and 3, and consequently improve the simulated temperature anomalies. An exception is over the Great Lakes, where the temperature anomalies are larger than surrounding land areas. The improvement in the large-scale atmospheric circulation and the resulting impact on the regional climate anomalies with nudging complements previous studies that used shorter simulations (Castro et al. 2005; Miguez-Macho et al. 2005; Bowden et al. 2012). The results show that the choice of nudging technique is less important than the decision to use interior nudging.

To provide further insight into the precipitation anomalies, the 850-hPa moisture transport and precipitable water anomalies are shown for the summer of 1993 and 2003 (Fig. 10). The observed precipitable water anomalies are as much as 5 mm day⁻¹ for JJA over parts of the Midwest during 1993, and a large component of this moisture is due to transport from the Gulf of Mexico (Fig. 10a). Accurately modeling the anticyclonic anomaly over the Southeast must be complemented with correctly simulating the precipitable water anomalies in order to capture the observed precipitation anomalies. The precipitable water anomalies are positive over the western portions of the Southeast (Arkansas, Mississippi, and Alabama) and decrease toward the east (North Carolina, South Carolina and Georgia), which is consistent with the larger negative precipitation anomalies simulated in the east (Fig. 8a). The precipitation anomalies in 2003 result from a significantly different

atmospheric circulation and provide additional evidence of the necessity for interior nudging to capture anomalies in both circulation and precipitation. During 2003 there is a stronger moisture flux component from the Gulf of Mexico for the Southeast (Fig. 10e), which generates positive precipitable water anomalies. This increase in moisture, in conjunction with an anomalous cyclonic circulation, contributes to the observed positive precipitation anomalies for the Southeast. The gradient in the precipitable water anomalies, from positive over the Southeast to negative over the Midwest and Plains, is consistent with the positive and negative precipitation anomalies for those respective regions.

The 1993 precipitable water anomalies and 850-hPa moisture transport for the NN, AN, and SN simulations are shown in Fig. 10b, c, and d, respectively. The NN anomalous low-level jet is consistent with observations except that the origin of the jet over the Gulf of Mexico has a stronger easterly component in NN. The difference in the moisture transport over the Gulf of Mexico in NN is a consequence of improperly simulating the large-scale anticyclonic anomaly over the Atlantic Ocean. The difference in the low-level circulation between NN and NARR results in maximizing moisture transport and convergence within the Southeast (northern Arkansas) in NN instead of in the Midwest. The observations indicate that the maximum precipitation anomaly coincides with the maximum precipitable water anomaly, but the maximum precipitation anomaly in NN is located much farther north than in the observations (Fig. 8). The AN and SN simulations improve the simulated easterly component of the moisture transport associated with the low-level jet compared with NN during 1993. Improvements in the moisture transport lead to a concentration of moisture over the Midwest for both simulations that used interior nudging. AN provides a better estimate of the magnitude of the precipitable water anomalies and their placement than SN, with higher precipitable water amounts extending towards the Gulf Coast. That extension of the positive precipitable water anomalies explains differences between AN and SN precipitation anomalies, as SN is much drier along the Gulf Coast.

The simulated precipitable water anomalies and 850-hPa moisture transport for the NN, AN, and SN simulations during summer 2003 are shown in Fig. 10f, g, and h, respectively. The 2003 NN simulation does not capture the moisture flux anomaly from the Gulf of Mexico into the Southeast. This can be partly explained by the momentum transfer of the stronger upper-level cyclonic circulation, as seen at 500-hPa (Fig. 9f), to lower levels of the atmosphere favoring a more northerly wind component at lower levels. The northerly component cuts off moisture from the Gulf of Mexico, which is consistent with negative precipitable

Fig. 9 Same as Fig. 7 but for 500-hPa wind vector anomalies (m s^{-1})

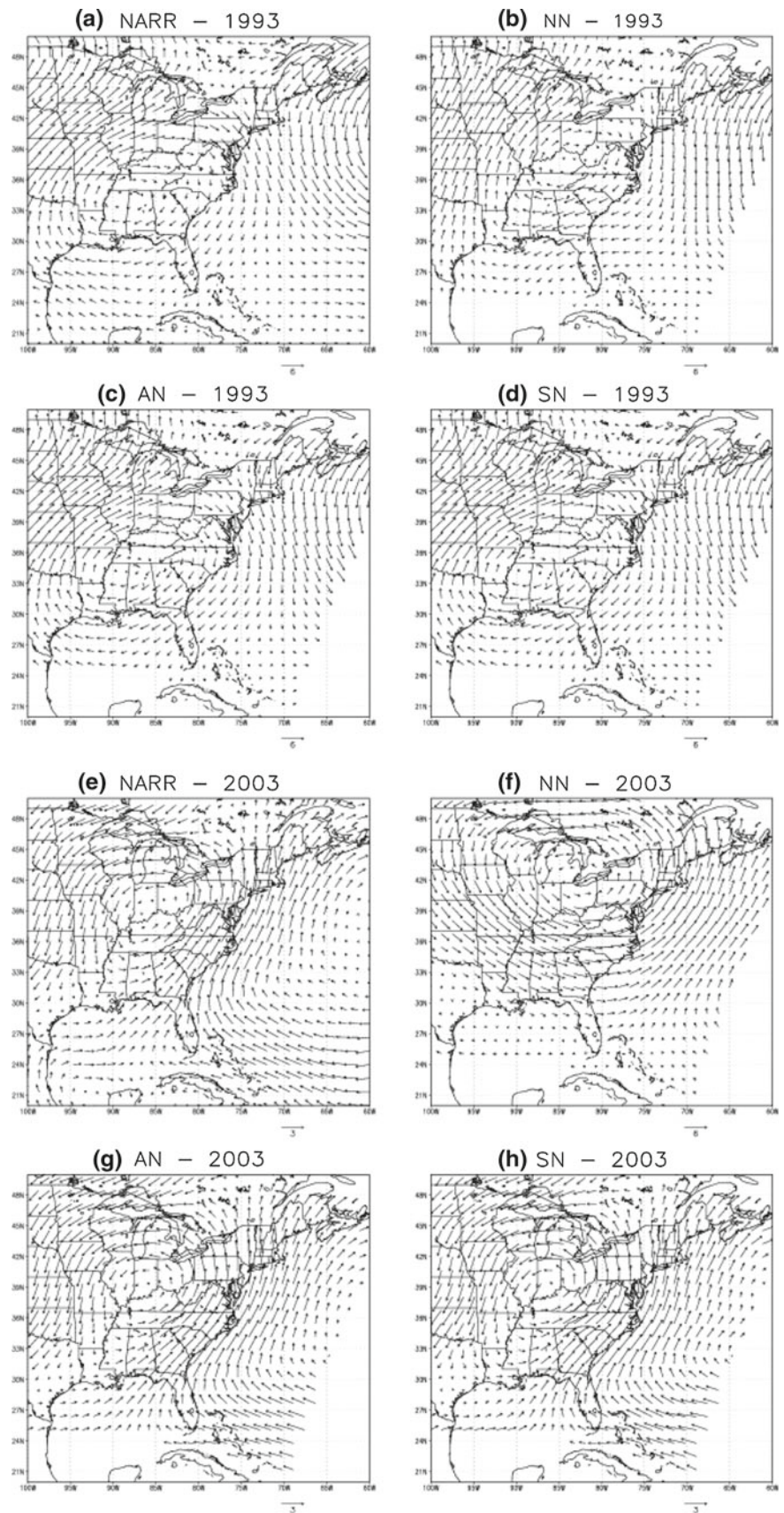
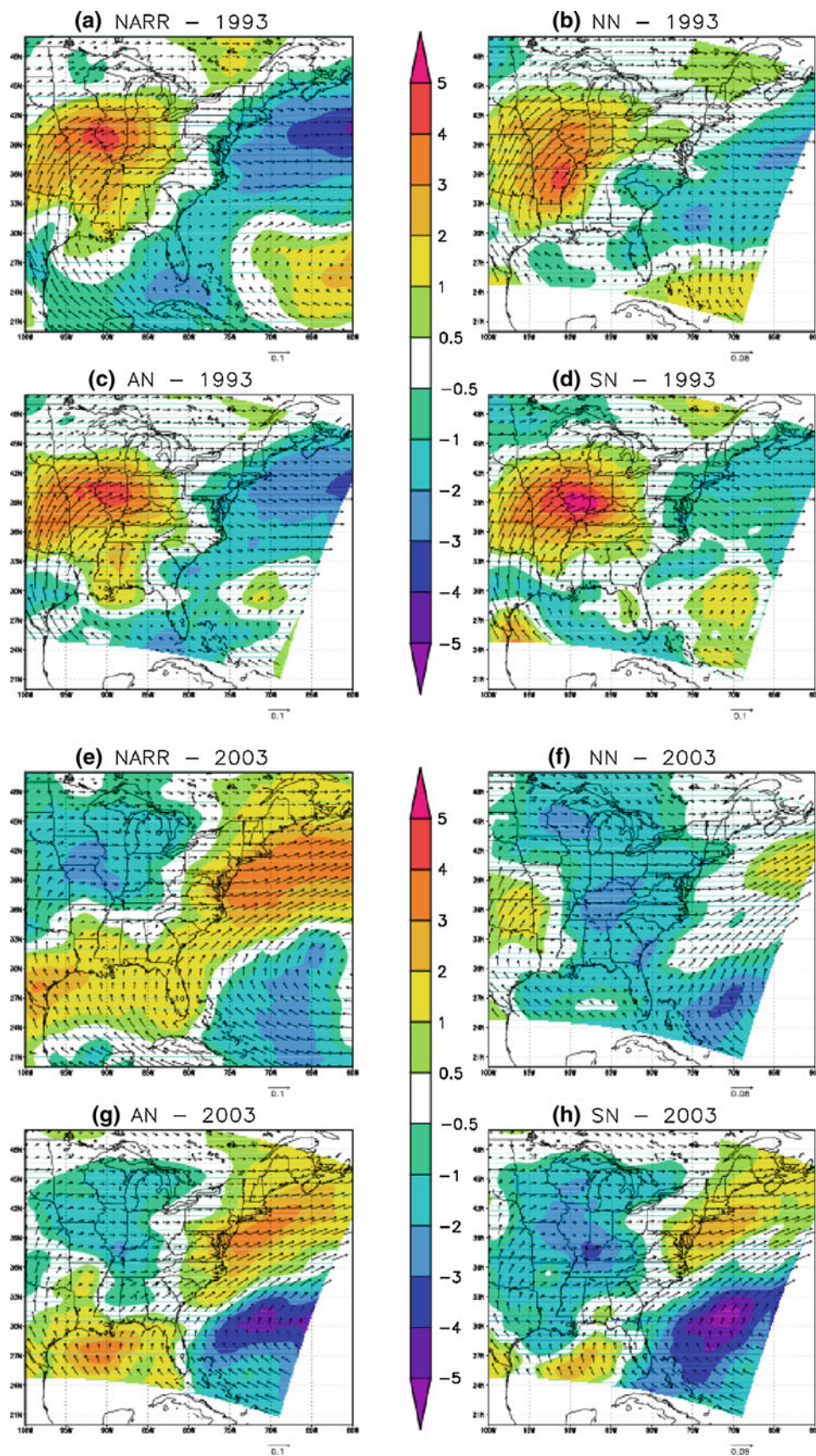


Fig. 10 Precipitable water anomaly (mm day^{-1} , shaded) with 850-hPa moisture transport anomaly (m/s) for the summer season for 1993 (top 4 panels) and 2003 (bottom 4 panels). The panels are labeled **a** NARR, **b** NN, **c** AN, **d** SN, **e** NARR, **f** NN, **g** AN, and **h** SN



water and precipitation anomalies over the Southeast, which are opposite from the observed anomalies, reducing the pattern correlation and increasing the RMSE. Here, again, errors in modeling the anomalous large-scale circulation in NN adversely impact the regional climate anomalies. AN and SN both successfully simulate the low-level moisture transport from the Gulf Coast up the eastern seaboard, but the positive precipitable water anomalies in AN agree better with observations. Tables 2 and 3 illustrate that the precipitable water anomalies are more than double in NN (1.7 mm day^{-1}) compared to AN (0.7 mm day^{-1}) with a pattern correlation increasing from 0.14 in NN to 0.87 in AN. Additionally, improvements in the precipitable water anomalies for AN compared to SN, as shown in Fig. 10 and Tables 2 and 3, suggests that nudging the moisture field may improve the accuracy of the simulated regional climate.

5 Summary

We examined the large-scale circulation in three continuous 20-year WRF simulations, one without interior grid nudging and two using different interior grid nudging methods. Examining the large-scale circulation was motivated by our application of WRF to downscale GCM output to examine the impacts of air quality under a changing climate. Without interior grid nudging, WRF may be inadequate to simulate the placement of the resolved large-scale circulation as represented by the GCM. In particular, the bias in 2-m temperature and precipitation is typically larger during the summer when air quality concerns related to ozone are important. We investigated whether errors in predicting the large-scale circulation strongly contributed to the large summer bias at the surface. The Bermuda high was identified as a large-scale circulation feature of interest because of its control on regional climate anomalies over the Southeast during the summer, its potential impact on air quality, and the observed/projected westward shift in the Bermuda high as the climate warms. This study illustrates problems that can arise in the large-scale circulation with weak constraint toward the driving fields.

The Bermuda high during the summer was first examined using the BHI to measure the intensity and anomalous placement of the Bermuda high. We found that the inter-annual variability in the intensity and placement of the Bermuda high is poorly simulated when no interior grid nudging is used. Both types of nudging drastically improved the representation of the BHI, which indicates that the large-scale circulation had been improved. Using the BHI, we identified two summers, 1993 and 2003, when the Bermuda high was anomalously west and east of its

climatological position. For these events we examined the impact on regional climate anomalies of 2-m temperature and precipitation with respect to the large-scale circulation. The NN 500-hPa wind vector anomalies for both summers indicate problems in simulating the proper placement of the large-scale atmospheric circulation anomalies. In 2003, there is an additional problem for NN as the anomalous circulation aloft is too strong, which may be transferring momentum to the lower atmosphere. This impacts the lower atmosphere by reducing the moisture transport and precipitable water affecting the convective environment and precipitation. Both interior grid nudging strategies greatly improve the representation of the large-scale circulation aloft and moisture transport/precipitable water anomalies helping to improve the sign and spatial distribution of the simulated 2-m temperature and precipitation anomalies. The results illustrate that weakly constraining the RCM to downscale GCM projections (as in NN) will likely misrepresent important large-scale shifts in the atmospheric circulation with respect to the Bermuda high and provide an unrealistic conceptual view of the regional climate change. Allowing the RCM large-scale circulation to deviate from the GCM should be avoided when faced with problems of modeling the large-scale circulation in the contemporary climate.

Although both nudging strategies result in improved simulation of large-scale circulation, there are differences in the regional climate anomalies for 2-m temperature and precipitation between the two nudging strategies. The differences in 2-m temperature and precipitation between AN and SN are generally local. The similarities in the large-scale environment indicate that local processes such as evaporation or cloud cover or embedded model biases from the LSM or PBL physics schemes likely contribute to these differences. We are currently further investigating the role of local processes with particular interest in the impact of nudging towards moisture. In addition, using the same modeling period as was used here, Otte et al. (2012) showed that nudging improved the prediction of extremes. Overall, these results suggest that more research is needed to further understand the impact of interior grid nudging for mesoscale and local processes that are associated with added value within RCMs. Regardless, using an interior constraint toward the driving model (such as with nudging) is recommended to correctly simulate the large-scale circulation in the RCM.

Acknowledgments The author's time at the EPA was supported by post-doctoral training opportunities managed by the National Research Council and the Oak Ridge Institute for Science and Education. Robert Gilliam and S.T. Rao (US EPA) provided technical feedback on this paper. The critique of the anonymous reviewers served to strengthen this manuscript. The US Environmental Protection Agency through its Office of Research and Development funded

and managed the research described here. It has been subjected to the Agency's administrative review and approved for publication.

References

- Alexandru A, de Elia R, Laprise R (2007) Internal variability in regional climate downscaling at the seasonal scale. *Mon Wea Rev* 135(9):3221–3238
- Anderson CJ, Arritt RW, Pan Z, Takle ES, Gutowski WJ, Otieno FO, da Silva R, Caya D, Christensen JH, Lüthi D, Gaertner MA, Gallardo C, Giorgi F, Laprise R, Hong SY, Jones C, Juang HM, Katzfey JJ, McGregor JL, Lapenta WM, Larson JW, Taylor JA, Liston GE, Pielke RA, Roads JO (2003) Hydrological processes in regional climate model simulations of the Central United States flood of June–July 1993. *J Hydro-meteor* 4(3):584–598
- Bowden JH, Otte TL, Nolte CG, Otte MJ (2012) Examining interior grid nudging techniques using two-way nesting in the WRF model for regional climate modeling. *J Clim* 25:2805–2823
- Bukovsky MS, Karoly DJ (2009) Precipitation simulations using WRF as a nested regional climate model. *J Appl Meteor Climatol* 48(10):2152–2159. doi:10.1175/2009JAMC2186.1
- Castro CL, Pielke RA, Leoncini G (2005) Dynamical downscaling: assessment of value retained and added using the regional atmospheric modeling system (RAMS). *J Geophys Res* 110: D05,108+
- Chen F, Dudhia J (2001) Coupling an advanced land surface hydrology model with the Penn State NCAR MM5 modeling system. Part I: model implementation and sensitivity. *Mon Wea Rev* 129(4):569–585
- Christensen J, Carter T, Rummukainen M, Amanatidis G (2007) Evaluating the performance and utility of regional climate models: the PRUDENCE project. *Climatic Change* 81(0):1–6
- Christensen JH, Machenhauer B, Jones RG, Schär C, Ruti PM, Castro M, Visconti G (1997) Validation of present-day regional climate simulations over Europe: LAM simulations with observed boundary conditions. *Clim Dyn* 13:489–506
- Collins WD, Rasch PJ, Boville BA, Hack JJ, McCaa JR, Williamson DL, Kiehl JT, Briegleb B, Bitz C, Lin SJ, Zhang M, Dai Y (2004) Description of the NCAR community atmosphere model (CAM 3.0). Tech. rep., NCAR Technical Note
- Davies HC (1976) A lateral boundary formulation for multi-level prediction models. *Q J Roy Meteor Soc* 102:405–418
- Giorgi F (2006) Regional climate modeling: status and perspectives. *J de Physique IV* 139:101–118
- Grell GA, Dévényi D (2002) A generalized approach to parameterizing convection combining ensemble and data assimilation techniques. *Geophys Res Lett* 29(14):1693+
- Grotch SL, MacCracken MC (1991) The use of general circulation models to predict regional climatic change. *J Clim* 4:286–303
- Hong SY, Lim JOJ (2006) The WRF single-moment 6-class microphysics scheme (WSM6). *J Korean Meteor Soc* 42(2): 129–151
- Hong SY, Noh Y, Dudhia J (2006) A new vertical diffusion package with an explicit treatment of entrainment processes. *Mon Wea Rev* 134(9):2318–2341
- Inatsu M, Kimoto M (2009) A scale interaction study on East Asian cyclogenesis using a general circulation model coupled with an interactively nested regional model. *Mon Wea Rev* 137(9):2851–2868
- Jones RG, Murphy JM, Noguer M (1995) Simulation of Climatic Change over Europe using a nested regional-climate model. I: assessment of control climate, including sensitivity to location of lateral boundaries. *Q J R Meteorol Soc* 121(526):1413–1449
- Kanamitsu M, Ebisuzaki W, Woollen J, Yang SK, Hnilo JJ, Fiorino M, Potter GL (2002) NCEP-DOE AMIP-II reanalysis (R-2). *Bull Am Meteorol Soc* 83:1631–1643
- Katz RW, Parlange MB, Tebaldi C (2003) Stochastic modeling of the effects of large-scale circulation on daily weather in the Southeastern US. *Climatic Change* 60(1):189–216
- Kida H, Koide T, Sasaki H, Chiba M (1991) A new approach to coupling a limited area model with a GCM for regional climate simulation. *J Meteor Soc Japan* 69:723–728
- Koster RD, Dirmeyer PA, Guo Z, Bonan G, Chan E, Cox P, Gordon CT, Kanae S, Kowalczyk E, Lawrence D, Liu P, Lu CH, Malyshev S, McAvaney B, Mitchell K, Mocko D, Oki T, Oleson K, Pitman A, Sud YC, Taylor CM, Verseghy D, Vasic R, Xue Y, Yamada T (2004) Regions of strong coupling between soil moisture and precipitation. *Science* 305(5687):1138–1140
- Laprise R, de-Elia R, Caya D, Biner S, Lucas-Picher P, Diaconescu E, Leduc M, Alexandru A, Separovic L (2007) Challenging some tenets of regional climate modelling. *Meteor Atmos Phys* 100:3–22
- Leung LR, Qian Y (2009) Atmospheric rivers induced heavy precipitation and flooding in the western US simulated by the WRF regional climate model. *Geophys Res Lett* 36(3):L03,820+
- Li W, Li L, Fu R, Deng Y, Wang H (2010) Changes to the North Atlantic subtropical high and its role in the intensification of summer rainfall variability in the Southeastern United States. *J Climate* 24(5):1499–1506
- Liu Kb, Fearn ML (2000) Reconstruction of prehistoric landfall frequencies of catastrophic Hurricanes in Northwestern Florida from Lake Sediment records. *Quatern Res* 54(2):238–245
- Lo JC, Yang Z, Pielke RA (2008) Assessment of three dynamical climate downscaling methods using the Weather Research and Forecasting (WRF) model. *J Geophys Res* 113(D9):D09,112+
- Lorenz P, Jacob D (2005) Influence of regional scale information on the global circulation: a two-way nesting climate simulation. *Geophys Res Lett* 32(18):L18,706+
- Lucas-Picher P, Caya D, de Elia R, Laprise R (2008) Investigation of regional climate models' internal variability with a ten-member ensemble of ten years over a large domain. *Clim Dyn* 31: 927–940
- Mesinger F, DiMego G, Kalnay E, Mitchell K, Shafran PC, Ebisuzaki W, Jović D, Woollen J, Rogers E, Berbery EH, Ek MB, Fan Y, Grumbine R, Higgins W, Li H, Lin Y, Manikin G, Parrish D, Shi W (2006) North American regional reanalysis. *Bull Am Meteor Soc* 87(3):343–360
- Miguez-Macho G, Stenchikov GL, Robock A (2004) Spectral nudging to eliminate the effects of domain position and geometry in regional climate model simulations. *J Geophys Res* 109:D13,104+
- Miguez-Macho G, Stenchikov GL, Robock A (2005) Regional climate simulations over North America: interaction of local processes with improved large-scale flow. *J Clim* 18(8):1227–1246
- Nigam S, Ruiz-Barradas A (2006) Seasonal hydroclimate variability over North America in global and regional reanalyses and AMIP simulations: varied representation. *J Climate* 19(5):815–837
- Otte TL, Nolte CG, Otte MJ, Bowden JH (2012) Does nudging squelch the extremes in regional climate modeling? *J Climate* (in press). doi:10.1175/JCLI-D-12-00048.1
- Pal JS, Eltahir EAB (2002) Teleconnections of soil moisture and rainfall during the 1993 midwest summer flood. *Geophys Res Lett* 29(18):1865+
- Pielke RA, Wilby D, Niyogi F, Hossain F, Daruku K, Adegoke J, Kallos G, Seastedt T, Sudig K (2011) Dealing with complexity and extreme events using a bottom-up, resource based vulnerability perspective. *AGU Monograph*. doi:10.1029/2011GM001086

- Robertson AW, Ghil M (1999) Large-scale weather regimes and local climate over the Western United States. *J Climate* 12(6):1796–1813
- Sanchez-Gomez E, Somot S, Déqué M (2009) Ability of an ensemble of regional climate models to reproduce weather regimes over Europe-Atlantic during the period 1961–2000. *Clim Dyn* 33(5):723–736
- Seager R, Murtugudde R, Naik N, Clement A, Gordon N, Miller J (2003) Air-sea interaction and the seasonal cycle of the subtropical anticyclones. *J Clim* 16:1948–1966
- Skamarock WC, Klemp JB, Dudhia J, Gill DO, Barker M, Duda KG, Huang XY, Wang W, Powers JG (2008) A description of the advanced research WRF version 3. Tech. rep. National Center for Atmospheric Research
- Stauffer DR, Seaman NL (1994) Multiscale four-dimensional data assimilation. *J App Meteor* 33:416–434
- von Storch H, Langenberg H, Feser F (2000) A spectral nudging technique for dynamical downscaling purposes. *Mon Weather Rev* 128:3664–3673
- Trenberth KE, Guillemot CJ (1996) Physical processes involved in the 1988 drought and 1993 floods in North America. *J Climate* 9:1288–1298
- Veljovic K, Rajkovic B, Fennessy MJ, Altshuler EL, Mesinger F (2010) Regional climate modeling: Should one attempt improving on the large scales. Lateral boundary condition scheme: any impact. *Meteorologische Zeitschrift* 19(3):237–246
- Waldron K, Peagle J, Horel J (1996) Sensitivity of a spectrally filtered and nudged limited area model to outer model options. *Mon Wea Rev* 124:529–547
- Wang C, Enfield DB (2001) The Tropical Western Hemisphere warm pool. *Geophys Res Lett* 28(8)
- Wang Y, Leung R, McGregor J, Lee DK, Wang WC, Kimura F (2004) Regional climate modeling: progress, challenges, and prospects. *J Meteor Soc Jap* 82(6):1599–1628
- Yhang YB, Hong SY (2011) A study on large-scale nudging effects in regional climate model simulation. *Asia-Pacific J Atmos Sci* 47(3):235–243